Supplemental Material: Phase driving hole spin qubits

Stefano Bosco,[1, *] Simon Geyer,[1] Leon C. Camenzind,[1, †] Rafael Eggli,[1] Andreas Fuhrer,[2] Richard J. Warburton,[1] Dominik M. Zumbühl,[1] J. Carlos Egues,[1, 3] Andreas V. Kuhlmann,[1] and Daniel Loss[1]

[1]*Department of Physics, University of Basel, Klingelbergstrasse 82, 4056 Basel, Switzerland*
[2]*IBM Research Europe-Zurich, Säumerstrasse 4, CH-8803 Rüschlikon, Switzerland*
[3]*Instituto de Física de São Carlos, Universidade de São Paulo, 13560-970 São Carlos, São Paulo, Brazil*

Here we show additional measurements of our two phase-driven hole spin qubits in two different devices. We also provide a derivation of the suppression of the main Rabi oscillations and the emergence of sidebands due to simultaneous phase and Rabi drives. Finally, we discuss in detail the noise resilience of the fundamental Rabi oscillations upon phase driving based on Floquet theory.

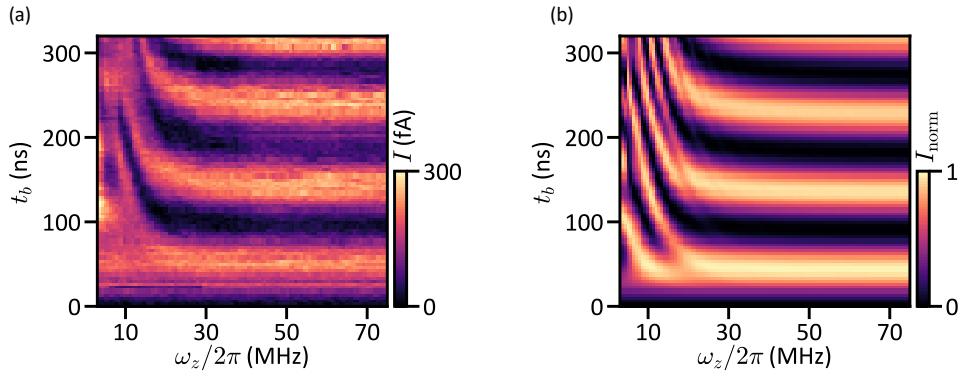## I. ADDITIONAL MEASUREMENTS OF OUR FIRST AND SECOND DEVICES

Figure 1. Phase-driving-induced slowing down of Rabi oscillations in qubit 2 (Q2). Measurements (a) and simulations (b) match well, similarly to the case reported in the main text for Q1; see Fig. 1(b),(c). Here $\omega_x/2\pi = \omega_q/2\pi = 3.115$ GHz, $\lambda_x/2\pi = 11$ MHz, and $\lambda_z/2\pi = 6.1$ MHz.
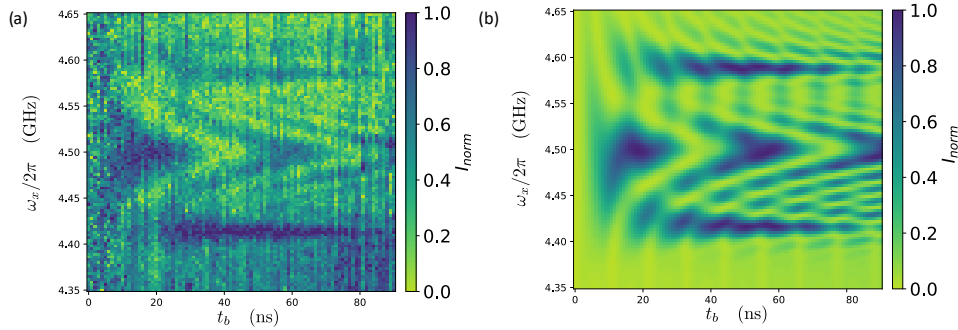

Figure 2. Phase-driving-induced sideband Rabi oscillations in qubit 1 (Q1). Measurements (a) and simulations (b) are in good agreement. These sidebands are analogous to the ones reported in the main text for Q2, see Fig. 2(b),(e). Here $\omega_q/2\pi = 4.5$ GHz, $\lambda_x/2\pi = \lambda_z/2\pi = 30$ MHz, and $\omega_z/2\pi = 90.5$ MHz, corresponding to $Z = 0.33$.

Here we present here additional data from our two qubits, Q1 and Q2, encoded in two different devices. In Fig. 1, we show the slowing down of Rabi oscillations by phase driving Q2. Compared to Figs. 1(b),(c) in the main text, we observe a similar trend, with lower Rabi and phase driving amplitudes. The measurement in Fig. 1(a) matches

well the numerical simulation in Fig. 1(b). In Fig. 2, we show phase-driving-induced sideband oscillations appearing at finite detuning in Q1. These results are similar to the ones for Q2 shown in Figs. 2(b),(e) of the main text. We observe a good agreement between measurements (a) and simulations (b).

II. DYNAMICS OF THE PHASE-DRIVEN QUBIT

Here we present a more detailed analysis of the sideband Rabi resonances and discuss the origin of the noise resilience for phase-driven qubits within the Floquet formalism.

A. Two-tone Hamiltonian

We consider the two-tone Hamiltonian

$$H = \frac{\hbar\omega_q}{2}\sigma_z + \hbar\lambda_x\sigma_x\cos(\omega_x t + \varphi_x) + \hbar\lambda_z\sigma_z\cos(\omega_z t + \varphi_z) \ , \tag{1}$$

with arbitrary phase shifts $\phi_{x,z}$. Equation (1) is slightly more general than Eq. (1) in the main text for which $\phi_x = \phi_z = 0$. Moving to the rotating frame defined by the transformation

$$U_r(t) = e^{-i\sigma_z[\omega_x t + \varphi_x + 2Z\sin(\omega_z t + \varphi_z)]/2} \ , \quad \text{with} \ \ Z = \lambda_z/\omega_z \ , \tag{2}$$

results in the effective Hamiltonian

$$\tilde{H} = \frac{\hbar\Delta}{2}\sigma_z + \frac{\hbar\lambda_x}{2}\left[e^{2iZ\sin(\omega_z t + \varphi_z)} + e^{2i[\omega_x t + \varphi_x + Z\sin(\omega_z t + \varphi_z)]}\right]\sigma_+ + \text{h.c.} \approx \frac{\hbar\Delta}{2}\sigma_z + \frac{\hbar\lambda_x}{2}e^{2iZ\sin(\omega_z t + \varphi_z)}\sigma_+ + \text{h.c.} \ , \tag{3}$$

with $\sigma_\pm = (\sigma_x \pm i\sigma_y)/2$ and $\Delta = \omega_q - \omega_x$. The approximate sign in Eq. (3) indicates a rotating wave approximation (RWA), valid when the phase driving frequency is much smaller than the transverse driving frequency, i.e. $\omega_z \ll \omega_x$. This is the regime of interest in our work; additional resonances can be found when $\omega_x \sim \omega_z$, and these effects are discussed in Ref. [1]. We also point out that Eq. (3) coincides with Eq. (2) in the main text. This can be shown by using the equalities

$$e^{2iZ\sin(\omega_z t + \varphi_z)} = \sum_{n=-\infty}^{\infty} e^{in(\omega_z t + \varphi_z)}J_n(2Z) \ , \quad \text{and} \ \ J_n(2Z) = (-1)^n J_{-n}(2Z) \ . \tag{4}$$

Note that at $Z = 0$ (corresponding to no phase driving $\lambda_z = 0$) we recover the usual Rabi Hamiltonian in the rotating frame and in the RWA,

$$\tilde{H}(Z = 0) = \frac{\hbar\Delta}{2}\sigma_z + \frac{\hbar\lambda_x}{2}\sigma_x \ , \tag{5}$$

as expected from Eq. (1) (see discussion Following Eq. (2) in the main text). On the other hand at $Z \to \infty$ (corresponding to $\omega_z = 0$), we find a constant shift of the qubit frequency by $2\lambda_t\cos(\varphi_z)$ resulting in a over-rotation of the driving term

$$\tilde{H}(Z \to \infty) = \frac{\hbar\Delta}{2}\sigma_z + \frac{\hbar\lambda_x}{2}e^{2i\lambda_z\cos(\varphi_z)t}\sigma_+ + \text{h.c.} \ . \tag{6}$$

Upon a transformation back to the lab frame, Eq. (6) reduces to the $\omega_z = 0$ of Eq. (1), as can be readily checked. We also remark that in taking the $Z \to \infty$ limit, we removed the divergent exponential $e^{2iZ\sin(\varphi_z)}$ by the trivial time-independent coordinate transformation $e^{iZ\sin(\varphi_z)\sigma_z}$, which does not affect the dynamics of the system.

B. Sideband Rabi resonances

We begin by examining the qubit dynamics when $\lambda_x \ll \omega_z$. In this case, only the lowest order Bessel functions in Eq. (4) determine the time-evolution of the qubit. As discussed in the main text, at $\Delta = 0$ the dominant contribution to the dynamics comes from the static term and results in a Rabi frequency $\omega_R = \lambda_x J_0(2Z)$; consequently for small phase-driving amplitudes $\lambda_z \ll \omega_z$, the Rabi oscillations are slowed down as $\omega_R \approx \lambda_x(1 - \lambda_z^2/\omega_z^2)$. Additional sideband
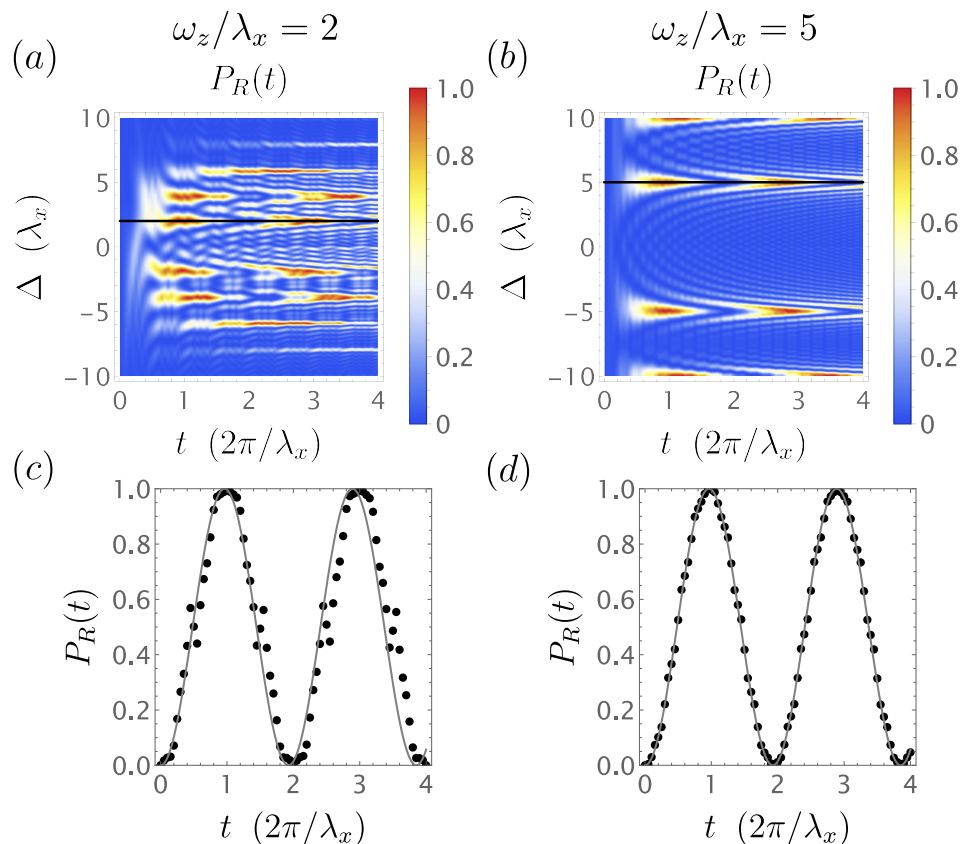
Figure 3. Additional simulations of sideband Rabi oscillations. Here we fix $Z = \lambda_z/\omega_z = 1.2$ such that the central Rabi resonance at $\Delta = 0$ vanishes. In (a) and (b) we use $\omega_z = 2\lambda_x$ (similar to our current experiments) and $\omega_z = 5\lambda_x$, respectively. We note that because the sidebands have a bandwidth $\sim \lambda_x$ and occur at frequencies $m\omega_z$, with integer m, they become increasingly well-resolved as the ratio ω_z/λ_x increases. This effect is illustrated in (c) and (d), where we show the first subband oscillations for the two different values of ω_z/λ_x, corresponding to the black lines in (a) and (b), respectively. For reference, we also show (gray line) the expected value of these oscillations $\sin^2[\lambda_x J_1(2.4)t/2]$. In (c) we observe additional wiggles in the vicinity of $P_R(t) \approx 0.5$ that are caused by corrections beyond the RWA. These corrections are suppressed in (d) and become negligible at larger values of λ_z. For the simulations we used $\omega_q = 10^3\lambda_x$.

Rabi oscillations appear at $\Delta = m\omega_z$ with frequency $\lambda_x J_m(2Z)$. Because the central contribution at $\Delta = 0$ vanishes at $Z \approx 1.2$ (root of $J_0(2Z)$), the dynamics becomes dominated by higher harmonic components. This condition has been realized in the experiments presented in the main text.

In Fig. 3, we report additional simulations for our system at $Z = \lambda_z/\omega_z = 1.2$, but for different values of ω_z. Because the sidebands have a bandwidth $\sim \lambda_x$, as the ratio ω_z/λ_x increases they become increasingly well separated in frequency and approach the ideal function $P_R(t) = \sin^2[\lambda_x J_1(2.4)t/2]$. For this reason, larger values of phase driving amplitude λ_z, such that the condition $Z = 1.2$ is fulfilled for larger frequencies ω_z, will enable high-fidelity sideband Rabi oscillations.

C. Floquet theory

We now consider a different case with $\lambda_x \sim \omega_z$ in which the higher harmonics become relevant also at $\Delta = 0$. The time-evolution operator of the system can be written in the form:

$$U(t) = U_r(t)U_{\text{TO}}(t)U_r^\dagger(0) , \quad \text{with} \quad U_{\text{TO}} = \mathcal{T}e^{-i\int_0^t d\tau \tilde{H}(\tau)/\hbar} , \tag{7}$$

where U_r is given in Eq. (2). Because in the RWA $\tilde{H}$ oscillates in time with period $T = 2\pi/\omega_z$, the time-ordered exponential in $U_{\text{TO}}(t)$ can be conveniently decomposed in the Floquet theory, see e.g. Ref. [2], as

$$U_{\text{TO}}(t) = e^{-iK(t)}e^{-iH_F t} . \tag{8}$$

We define the Floquet Hamiltonian H_F from the relation $e^{-iH_F T} = U_{\text{TO}}(T)$ and the kick operator as $e^{-iK(t)} = U_{\text{TO}}(t)e^{iH_F t}$. The usefulness of these operators is discussed below. This decomposition factorizes $U_{\text{TO}}(t)$ into a stroboscopic time-evolution operator dependent on H_F that captures the dynamics at times $t = nT$ and a kick operator satisfying $K(t) = K(t+T)$ that captures the dynamics within a single period. We also fix the Floquet gauge by specifying the initial condition of the kick operator $K(0) = 0$.

Using the decomposition in Eq. (8) we introduce the Floquet time-dependent modes

$$|\varphi_j(t)\rangle = e^{-i\omega_F^j t}|u_j(t)\rangle , \tag{9}$$

where the state $|u_j(t)\rangle$ is given by

$$|u_j(t)\rangle = e^{-iK(t)}|j_F\rangle , \tag{10}$$

and is periodic in time with period T, i.e. $|u_j(t)\rangle = |u_j(t + T)\rangle$. The $|\varphi_j(t)\rangle$ are analogous to Bloch states. The time-independent states $|j_F\rangle = |u_j(0)\rangle = |\varphi_j(0)\rangle$ and their quasi-energy ω_F^j [defined mod$(2\pi/T)$] are found from the eigensystem of the Floquet time-evolution operator $U_{\text{TO}}(T) = e^{-iH_F T}$:

$$U_{\text{TO}}(T)|j_F\rangle = e^{-i\omega_F^j T}|j_F\rangle . \tag{11}$$

The time-dependent states $|\psi(t)\rangle$ generated from $U_{\text{TO}}(t)$ can be decomposed in terms of Floquet time-dependent modes $|\varphi_j(t)\rangle$ as

$$|\psi(t)\rangle = U_{\text{TO}}(t)|\psi_0\rangle = \sum_j c_j|\varphi_j(t)\rangle . \tag{12}$$

The initial condition $|\psi(0)\rangle = |\psi_0\rangle$ enters via the time-independent coefficients c_j, obtained from the decomposition of the state $|\psi_0\rangle$ in the time-independent Floquet eigenbasis $|j_F\rangle$, i.e.,

$$c_j = \langle j_F|\psi_0\rangle . \tag{13}$$

Next we consider in detail the two cases studied in the main text, where the phase driving frequency ω_z is either off or on resonance with the Rabi frequency λ_x and the phase-driving amplitude λ_z is small compared to ω_z, i.e., $Z \ll 1$. In both cases, we assume that the transverse drive is resonant with the qubit frequency, i.e. $\Delta = 0$.

1. Off-resonant phase driving at $\lambda_x \ll \omega_z$

For small off-resonant phase-driving and assuming $Z \ll 1$ and $\Delta = 0$, Eq. (3) simplifies to

$$\tilde{H} \approx \frac{\hbar\lambda_x}{2}\sigma_x - \hbar\lambda_x Z \sin(\omega_z t + \varphi_z)\sigma_y . \tag{14}$$

Since the phase-driving frequency ω_z is much larger than λ_x, and we can use a Magnus expansion [3] to derive the effective time-evolution operator

$$U_{\text{TO}}(t) = e^{-i\frac{\lambda_x t}{2}\left[\sigma_x - 2Z\frac{\cos(\varphi_z) - \cos(\omega_z t + \varphi_z)}{\omega_z t}\sigma_y\right]} \text{ and Floquet Hamiltonian } H_F = \frac{\lambda_x}{2}\sigma_x . \tag{15}$$

This is similar to the case describing the usual Rabi oscillations in which we find that the two Floquet modes are coherent superpositions of the spin states, i.e.

$$|0_F\rangle = \frac{|\uparrow\rangle + |\downarrow\rangle}{\sqrt{2}} , \quad |1_F\rangle = \frac{|\uparrow\rangle - |\downarrow\rangle}{\sqrt{2}} \text{ and } \omega_F^{0,1} = \pm\frac{\lambda_x}{2} \text{ mod}(\omega_z) . \tag{16}$$

2. Resonant phase driving at $\lambda_x \sim \omega_z$

A different situation occurs at resonance $\lambda_x \sim \omega_z$ where the Magnus expansion is not applicable. Here we still consider $\Delta = 0$ and $Z \ll 1$. In this case, we first move to a doubly rotating frame by

$$U_1(t) = e^{-i(\omega_z t + \varphi_z)\sigma_x/2} , \tag{17}$$

that eliminates the usual Rabi oscillation term. We then obtain

$$H_1 = \frac{\hbar}{2} \left(\lambda_x - \omega_z\right) \sigma_x - \frac{\hbar \lambda_x Z}{2} \sigma_z + \frac{\hbar \lambda_x Z}{2} \left[\cos(2\omega_z t + 2\varphi_z)\sigma_z - \sin(2\omega_z t + 2\varphi_z)\sigma_y\right] \ , \tag{18}$$

where we can safely use a lowest-order Magnus expansion [3], because $\lambda_x Z \ll \omega_z$, to obtain the time-evolution operator

$$U_{\text{TO}}(t) = U_1(t) e^{-i\frac{(\lambda_x - \omega_z)t}{2}\sigma_x + i\frac{\lambda_x Z t}{2}\sigma_z + i\frac{\lambda_x Z t}{2}\frac{\sin(\omega_z t)}{\omega_z t}[\sin(\omega_z t + 2\varphi_z)\sigma_y - \cos(\omega_z t + 2\varphi_z)\sigma_z]} U_1^\dagger(0) \ . \tag{19}$$

At the stroboscopic time $t = T = 2\pi/\omega_z$, the time-evolution operator significantly simplifies and we can rewrite it as

$$U_{\text{TO}}(T) = U_1(T) e^{i\left(\theta - \frac{\pi}{4}\right)\sigma_y} e^{-i\frac{\tilde{\omega}_F T}{2}\sigma_z} e^{-i\left(\theta - \frac{\pi}{4}\right)\sigma_y} U_1^\dagger(0) \quad \text{with} \quad \tan(2\theta) = \frac{\lambda_x Z}{|\lambda_x - \omega_z|} \quad \text{and} \quad \tilde{\omega}_F = \sqrt{(\lambda_x - \omega_z)^2 + \lambda_x^2 Z^2} \ . \tag{20}$$

Diagonalizing $U_{\text{TO}}(T)$, by using the above we immediately find the Floquet eigensolutions

$$\omega_F^{0,1} = \pm \left(\frac{\omega_z}{2} + \frac{\tilde{\omega}_F}{2}\right) \text{mod}(\omega_z) \quad \text{and} \quad \langle s|j_F\rangle = \left[U_1(0)e^{i\left(\theta - \frac{\pi}{4}\right)\sigma_y}\right]_{s,j} \ , \quad \text{with} \quad s = \{\uparrow, \downarrow\} \ , \quad j_F = \{0_F, 1_F\} \ . \tag{21}$$

These equations correspond to Eqs. (4) and (5) in the main text up to an irrelevant global phase factor. As shown in the main text they agree well with the numerical solution obtained by computing the eigenvalues of the time-evolution operator of the Hamiltonian H in Eq. (1). We emphasize that the phases $\varphi_{x,z}$ can be used to prepare a coherent superposition of Floquet eigenstates (see Fig. 3 in the main text).

For small values of Z, we can also extend our model to include a finite detuning Δ between the transversal driving and the qubit frequency. In this case, the transformation $U_1(t)$ in Eq. (17) can be generalized to

$$U_1(t) \rightarrow U_1(t) = e^{-i\varepsilon\sigma_y} e^{-i(\omega_z t + \varphi_z)\sigma_x/2} \ , \tag{22}$$

with $\varepsilon = \arctan(\Delta/\lambda_x)/2$, where the additional term performs an initial rotation of the state to include the detuning. This transformation modifies only the first term of the Hamiltonian H_1 in Eq. (23) as

$$\frac{\hbar}{2} \left(\lambda_x - \omega_z\right) \sigma_x \rightarrow \frac{\hbar}{2} \left(\sqrt{\lambda_x^2 + \Delta^2} - \omega_z\right) \sigma_x \ , \tag{23}$$

and results in the Floquet eigensystem

$$\omega_F^{0,1} = \pm \left(\frac{\omega_z}{2} + \frac{\tilde{\omega}_F^\Delta}{2}\right) \text{mod}(\omega_z) \quad \text{and} \quad \langle s|j_F\rangle = \left[e^{-i\varepsilon\sigma_y} e^{-i\varphi_z\sigma_x/2} e^{i\left(\theta^\Delta - \frac{\pi}{4}\right)\sigma_y}\right]_{s,j} \ , \tag{24}$$

with renormalized quantities

$$\tan(2\theta^\Delta) = \frac{\lambda_x Z}{|\sqrt{\lambda_x^2 + \Delta^2} - \omega_z|} \quad \text{and} \quad \tilde{\omega}_F^\Delta = \sqrt{\left(\sqrt{\lambda_x^2 + \Delta^2} - \omega_z\right)^2 + \lambda_x^2 Z^2} \ . \tag{25}$$

First, we note that at small detuning the minimal Floquet band gap is shifted towards smaller values of $\lambda_x = \sqrt{\omega_z^2 - \Delta^2}$. Interestingly, the Floquet eigenstates coincide with the spin up and down states at a different value of λ_x, namely at $\lambda_x = \omega_z + Z\Delta$ when the Rabi and phase driving are in-phase $\varphi = 0$ and at $\lambda_x = \omega_z - Z\Delta$ when they are completely out-of-phase and $\varphi = \pi$.

3. Rabi oscillations

We now reinterpret our Rabi oscillations in terms of Floquet eigenmodes. When $|\psi_0\rangle = |\uparrow\rangle$, the spin flip probability is given by

$$P_R(t) = |\langle\downarrow|\psi(t)\rangle|^2 = 1 - |\langle\uparrow|\psi(t)\rangle|^2 = 1 - \left|\sum_{jj'} c_j c_{j'}^* e^{-i\omega_F^j t} \langle j_F'|u_j(t)\rangle\right|^2 \ . \tag{26}$$

Focusing on the stroboscopic evolution, we find at times nT, with integer n,

$$P_R(nT) = 1 - \left| \sum_j |c_j|^2 e^{-in\omega_F^j T} \right|^2 = \sin^2(\Theta)\sin^2(\tilde{\omega}_F nT) \ , \tag{27}$$

where in the last line we introduced a convenient parametrization of the coefficients $|c_0|^2 = \cos^2(\Theta/2)$ and $|c_1|^2 = \sin^2(\Theta/2)$, as well as the frequency gap $\tilde{\omega}_F = (\omega_F^0 - \omega_F^1)/2$.

For a weak off-resonant phase driving $\omega_z \gg \lambda_x$, $Z \ll 1$, and $\Delta = 0$, we obtain $\Theta = \pi/2$, corresponding to $|c_0|^2 = |c_1|^2 = 1/2$, i.e., equal probability of occupation of Floquet eigenmodes [see Eq. (16)]. In this case, we observe fully developed Rabi oscillations with period $2\tilde{\omega}_F = \lambda_x \ll \omega_q$.

However, when phase driving is resonant, i.e., $\omega_z = \lambda_x$, there is another possible way to obtain fully-developed Rabi oscillations. As shown in the main text, phase driving with $\varphi_x = \varphi_z = 0$ enables the case $\Theta = 0$ [or, equivalently, $\Theta = \pi$], see also Eq. (21), such that at $t = 0$ the single Floquet mode $|0_F\rangle = |\uparrow\rangle$ $[|1_F\rangle = |\downarrow\rangle]$ is prepared and

$$P_R(t) = |\langle\downarrow|\psi(t)\rangle|^2 = 1 - |\langle 0_F|u_0(t)\rangle|^2 = |\langle 1_F|u_0(t)\rangle|^2 \ . \tag{28}$$

Note that $u_0(t)$ is periodic with period $T = 2\pi/\omega_z$ and thus $P_R(nT) = 0$. The Rabi oscillations in this case directly probes the temporal structure of the Floquet eigenmode $u_0(t)$, and does not need to be sinusoidal, as shown in Fig. 3 of the main text. This distinction makes an important difference when noise is included.

D. Noisy Rabi oscillations

Here we discuss the effects of noise on our hole qubit and how phase driving can mitigate its effects.

1. Noise model and parameter estimates

We now discuss the possible noise sources in our device. We consider an ensemble of defects that produce a small random field $\mathbf{V}(t)$ coupling to the Zeeman and driving vectors as

$$H_N = \frac{\hbar\omega_q}{2}\boldsymbol{\eta}_q(t)\cdot\boldsymbol{\sigma} + \hbar\lambda_x\boldsymbol{\eta}_x(t)\cdot\boldsymbol{\sigma}\cos(\omega_x t + \varphi_x) + \hbar\lambda_z\boldsymbol{\eta}_z(t)\cdot\boldsymbol{\sigma}\cos(\omega_z t + \varphi_z) \ . \tag{29}$$

We introduce the dimensionless random vectors $\boldsymbol{\eta}_q(t) = \mathbf{V}(t)\partial_{\mathbf{V}}[\omega_q\mathbf{e}_z]/\omega_q$, $\boldsymbol{\eta}_x(t) = \mathbf{V}(t)\partial_{\mathbf{V}}[\lambda_x\mathbf{e}_x]/\lambda_x$, and $\boldsymbol{\eta}_z(t) = \mathbf{V}(t)\partial_{\mathbf{V}}[\lambda_z\mathbf{e}_z]/\lambda_z$ that describe the relative variations of Zeeman and driving vectors caused by the defects. In general cases, we expect the absolute values of the relative variations to be of the same order of magnitude and thus assume for simplicity $\boldsymbol{\eta}_q(t) = \boldsymbol{\eta}_x(t) = \boldsymbol{\eta}_z(t) \equiv \boldsymbol{\eta}(t) = [\eta_1(t), \eta_2(t), \eta_3(t)]$.

We also assume that the noise is isotropic and uncorrelated, such that $\langle\eta_i(t)\eta_j(0)\rangle = \delta_{ij}\int d\omega e^{-i\omega t}S(\omega)/2\pi$, where we introduced the noise spectral function $S(\omega)$. Because the fluctuations of the field $\mathbf{V}(t)$ produced by typical noise sources are peaked at low frequencies, below we will consider the two common cases of quasistatic $S_{\text{QS}}(\omega) = 4\pi\eta^2\delta(\omega)$ and pink noise, $S_{\text{PN}}(\omega) = \eta^2/|\omega|^{1-\epsilon}$, with $\epsilon \to 0$ and η being the average amplitude of the fluctuations.

In the rotating frame defined by $U_r(t)$ in Eq. (2), we find

$$\tilde{H}_N = \frac{\hbar\omega_q}{2}\left[\eta_3(t)\sigma_z + \eta_-(t)e^{i\omega_x t}e^{2iZ\sin(\omega_z t)}\sigma_+ + \text{h.c.}\right] \tag{30}$$

$$+ \frac{\hbar\lambda_x}{2}\left[2\eta_3(t)\cos(\omega_x t)\sigma_z + \eta_-(t)\left(1 + e^{2i\omega_x t}\right)e^{2iZ\sin(\omega_z t)}\sigma_+ + \text{h.c.}\right] \tag{31}$$

$$+ \frac{\hbar\lambda_z}{2}\left[2\eta_3(t)\cos(\omega_z t)\sigma_z + \eta_-(t)\left(e^{i(\omega_x - \omega_z)t} + e^{i(\omega_x + \omega_z)t}\right)e^{2iZ\sin(\omega_z t)}\sigma_+ + \text{h.c.}\right] \ , \tag{32}$$

where $\eta_\pm = \eta_1 \pm i\eta_2$ and we set $\varphi_x = \varphi_z = 0$ for simplicity.

Moving in the interaction picture by considering also the time-evolution operator U_{TO} in Eq. (7), we obtain

$$H_N^I = U_{\text{TO}}^\dagger(t)\tilde{H}_N U_{\text{TO}}(t) \equiv \frac{\mathbf{h}_N(t)\cdot\boldsymbol{\sigma}}{2} \ , \tag{33}$$

where we introduced the noise vector $\mathbf{h}_N(\tau)$. In the two cases of interest discussed in Sec. II C, i.e. the off-resonant ($\omega_z \gg \lambda_x$) and resonant ($\omega_z = \lambda_x$) cases, we find for $\omega_q \gg \omega_z$, $\Delta = 0$, and $Z \ll 1$, respectively,

$$\mathbf{h}_N^{\omega_z \gg \lambda_x} \approx \hbar\omega_q\Big(\eta_1\cos(\omega_q t) + \eta_2\sin(\omega_q t), \ \eta_3\sin(\lambda_x t), \ \eta_3\cos(\lambda_x t)\Big) \tag{34a}$$

$$+ \hbar\lambda_x\Big(\eta_1, \ \eta_2\cos(\lambda_x t), \ -\eta_2\sin(\lambda_x t)\Big) \tag{34b}$$

$$+ \hbar\lambda_z\Big(\eta_1\cos[(\omega_q-\omega_z)t] + \eta_2\sin[(\omega_q-\omega_z)t], \ \eta_3\sin[(\lambda_x-\omega_z)t], \ \eta_3\cos[(\lambda_x-\omega_z)t]\Big) , \tag{34c}$$

$$\mathbf{h}_N^{\omega_z = \lambda_x} \approx \hbar\omega_q\Big(-\eta_3\cos[(\lambda_x-\lambda_z)t]/2, \ \eta_3\sin[(\lambda_x-\lambda_z)t]/2, \ \eta_3\cos(\lambda_x t)\Big) \tag{34d}$$

$$+ \hbar\lambda_x\Big(\eta_1\cos(\lambda_z t), \ \eta_1\sin(\lambda_z t), \ -\eta_2\sin(\lambda_x t)\Big) \tag{34e}$$

$$+ \hbar\lambda_z\Big(-\eta_3\cos[(2\lambda_x-\lambda_z)t]/2, \ \eta_3\sin[(2\lambda_x-\lambda_z)t]/2, \ \eta_3\Big) , \tag{34f}$$

where we kept only the dominant components for each noise source, i.e. the ones oscillating at the lowest frequencies.

For small noise amplitudes, the total time-evolution operator for a single noise realization is well-approximated by a lowest-order Magnus exapansion [3] of the Hamiltonian H_N^I in the interaction picture. Going back to the lab frame, this expansion results in the operator

$$U_N(t) = U(t)e^{-i\boldsymbol{\phi}(t)\cdot\boldsymbol{\sigma}/2}U^\dagger(0) , \quad \text{with} \ \ \boldsymbol{\phi}(t) = \int_0^t d\tau\,\mathbf{h}_N(\tau)/\hbar , \tag{35}$$

describing the total time-evolution of the spin state including a single realization of noise.

Our current devices have a limited measurement-time window ≈ 2 μs that is determined by our dc transport readout technique. Within this window we do not observe visible decay of Rabi oscillations and thus we cannot precisely characterize T_2^R; this limitation can be overcome by dispersive readout techniques [4]. However, from our previous measurements in Ref. [5], we can still estimate T_2^R. In particular, noise with exponent $\epsilon \approx 0.1$ has been reported in our devices [5]. This exponent is measured at temperature ~ 1.5 K, and because ϵ shows a clear trend of decreasing at lower temperatures, and our current devices are operated ~ 100 mK, we expect $\epsilon \lesssim 0.1$. From the measured values of $T_2^* \sim 0.3$ μs [5], and by using the standard formula $T_2^* = \sqrt{2\pi\epsilon}/\omega_q\eta$ [6] with $\omega_q/2\pi = 8.8$ GHz [5], we estimate $\eta \approx 5 \times 10^{-5}$ in our current devices. We note that the estimated parameters agree with the value $T_2^{\text{CPMG}} \sim 1.5$ μs measured with two applied π-pulses [5]; we used in this case $T_2^{\text{CPMG}} \approx 4/\omega_q\eta$ [6].

We also remark that because in our devices $\epsilon \to 0$ at low temperatures, resulting in a noise spectrum that is strongly peaked at low frequencies, the quasi-static noise approximation discussed in the main text reasonably approximates the response of the system. For quasi-static noise, $\eta = 5 \times 10^{-5}$ results in a similar value of $T_2^* \approx 1/\omega_q\eta \approx 0.35$ ns.

2. Noise and Floquet eigenstates

The Floquet theory introduced in Sec. II C provides a convenient and straightforward framework to describe noisy Rabi oscillations. In terms of the Floquet eigenmodes in Eq. (12) and using Eq. (35), the time-evolved state for a single noise realization is given by

$$|\psi^N(t)\rangle = \sum_{jj'} |\varphi_j(t)\rangle \mathcal{D}_{jj'}(t)c_{j'} , \quad \text{with} \ \ \mathcal{D}_{jj'}(t) = \langle j_F|e^{-i\boldsymbol{\phi}(t)\cdot\boldsymbol{\sigma}/2}|j_F'\rangle , \tag{36}$$

resulting in the Rabi probability [see Eq. (26)]

$$P_R^N(t) = |\langle\downarrow|\psi^N(t)\rangle|^2 = 1 - \left|\sum_{jj'j''} c_j c_{j'}^* e^{-i\omega_F^{j''}t}\langle j_F'|u_{j''}(t)\rangle\mathcal{D}_{j''j}(t)\right|^2 . \tag{37}$$

As discussed below, the above formulation allows us to explain the phase-driving-induced enhancement of Rabi oscillations by considering the effect of dephasing and relaxation of Floquet eigenmodes.
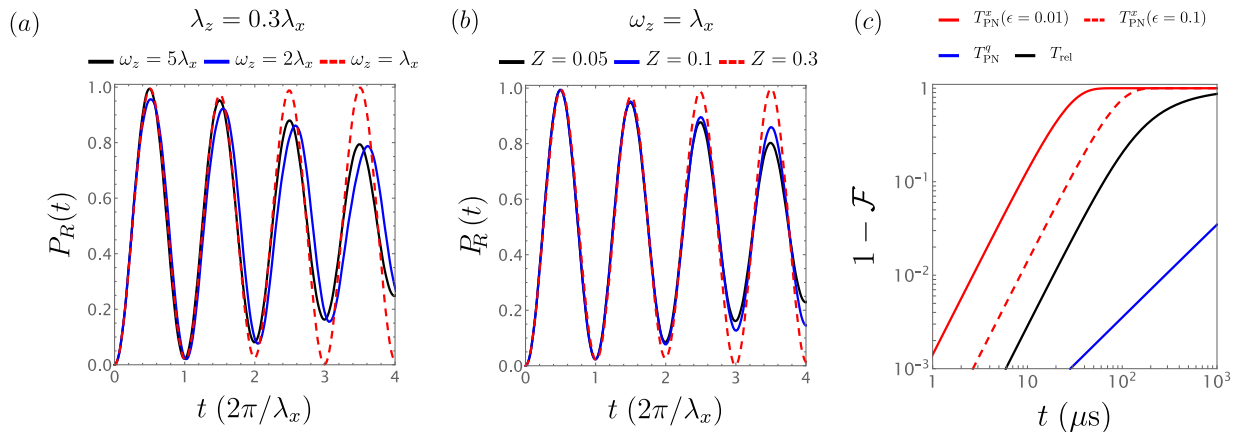
Figure 4. Decay of Rabi oscillations. (a) Decay of Rabi oscillations at fixed λ_z for several ratios ω_z/λ_x for quasi-static noise $S_{\mathrm{QS}}(\omega) \propto \delta(\omega)$. By adding a small phase drive satisfying $\omega_z = \lambda_x$, the attenuation of the Rabi oscillations can be suppressed. The results are obtained by numerically computing the time-evolution generated by the Hamiltonian in Eq. (1), with $\lambda_x = \lambda_z/0.3 = 2\pi \times 30$ MHz, $\omega_q = \omega_x = 10^3\lambda_x$, and $\varphi_x = \varphi_z = 0$. We include here only the leading term ($\propto \lambda_x$) of disorder in Eq. (29), and, consistently with the quasi-static noise approximation, we consider a Gaussian-distributed vector of random variables $\boldsymbol{\eta}$, with standard deviation $\sigma = 0.05$. Black, blue, and red lines in (a) are obtained for $\omega_z = 5\lambda_x$, $\omega_z = 2\lambda_x$, and $\omega_z = \lambda_x$, respectively. Note the slowdown of the damped Rabi oscillations (see blue and red lines). The results are obtained by averaging over 10^3 random realizations of noise. (b) Decay of Rabi oscillations at $\omega_z = \lambda_x$. By turning on phase driving, the decay of the Rabi oscillations can be controllably suppressed. The results are obtained at resonance $\lambda_x/2\pi = \omega_z/2\pi = 30$ MHz and by using $\omega_q = \omega_x = 10^3\lambda_x$, and $\varphi_x = \varphi_z = 0$ in analogy to (a). Black, blue, and red lines in (b) correspond to $\lambda_z = 0.05\lambda_x$, $\lambda_z = 0.1\lambda_x$, and $\lambda_z = 0.3\lambda_x$, respectively, and show that as the Floquet gap becomes larger than the noise ($\lambda_z \gtrsim \lambda_x\sigma$), Rabi oscillations are restored. (c) Double logarithmic plot of the infidelity $1 - \mathcal{F}$ of Rabi oscillations showing their decay due to dephasing and relaxation of Floquet eigenmodes and assuming pink noise $S_{\mathrm{PN}}(\omega) \propto 1/|\omega|^{1-\epsilon}$. Dephasing of the Floquet modes is the dominant cause of the decay of Rabi oscillations for $\omega_z \gg \lambda_x$. It comprises two leading contributions estimated in Sec. II D 3. The red solid (dashed) line corresponds to the Gaussian decay $\mathcal{F} = e^{-[t/T_{\mathrm{PN}}^x]^2}$, with $T_{\mathrm{PN}}^x = 25$ μs ($T_{\mathrm{PN}}^x = 85$ μs) obtained for the low (high) temperature estimation of ϵ, see Eqs. (43) and (44). The blue line shows the slower exponential decay $\mathcal{F} = e^{-t/T_{\mathrm{PN}}^q}$ with $T_{\mathrm{PN}}^q \sim 28$ ms. These contributions do not affect the qubit when a sufficiently large phase driving is applied at $\omega_z = \lambda_x$. In this case, the decay is determined by relaxation between Floquet eigenmodes (black line), with $\mathcal{F} \sim 1/\sqrt{1 + (4t/T_{\mathrm{rel}})^2}$, and $T_{\mathrm{rel}} = 530$ μs, see Eqs. (46) and (48).

3. Dephasing of Floquet modes

We first focus on pure dephasing of Floquet modes and consider $\mathcal{D}_{ij}^{\mathrm{deph}}(t) = \delta_{ij}e^{-i\phi_j(t)/2}$. In this simple case, the Rabi probability simplifies to

$$P_R^N(t) = 1 - \left| \sum_{jj'} c_j c_{j'}^* e^{-i\omega_F^j t} \langle j_F' | u_j(t) \rangle e^{-i\phi_j(t)/2} \right|^2 . \tag{38}$$

In conventional Rabi experiments, dephasing dominates the decay of the oscillations. We now distinguish between the off-resonant phase driving ($\omega_z \gg \lambda_x$), where the Floquet modes are equally populated, and the resonant phase driving ($\omega_z = \lambda_x$), where a single Floquet mode is occupied [see the discussion in Sec. II C]. In these two cases, $\mathcal{D}^{\mathrm{deph}}(t)$ accounts for the noise contributions $[\mathbf{h}_N^{\omega_z \gg \lambda_z}]_x$ and $[\mathbf{h}_N^{\omega_z = \lambda_z}]_z$ in Eq. (34), respectively.

a. Off-resonant phase driving $\omega_z \gg \lambda_z$. From the discussion in Sec. II C 3, when $\omega_z \gg \lambda_x$, here the Floquet modes are equally populated. By defining $\phi(t) = (\phi_0(t) - \phi_1(t))/2$, the Rabi probability for a single disorder realization at the stroboscopic times nT reduces to [see Eq. (27)]

$$P_R^N(nT) = \sin^2\left[\frac{\lambda_x nT + \phi(nT)}{2} \right] . \tag{39}$$

Assuming a usual Gaussian distribution of the phase with standard deviation $\sigma(nT)$ and zero mean-value, we obtain after averaging over many realizations

$$\langle P_R^N(nT) \rangle = \frac{1}{2} - \frac{1}{2}e^{-\frac{\sigma^2(nT)}{2}}\cos(\lambda_x nT) . \tag{40}$$

The exponential factor $e^{-\sigma^2(nT)/2}$ causes the conventional decay of Rabi oscillations. In this case, we find

$$\sigma^2(nT) \approx \frac{1}{2\pi} \int_{-\infty}^{\infty} d\omega S(\omega) \Big[\lambda_x^2 f(\omega, 0, nT) + \omega_q^2 f(\omega, \omega_q, nT) + \lambda_z^2 f(\omega, \omega_q - \omega_z, nT)\Big] , \tag{41}$$

where we introduce the function

$$f(\omega, \omega_q, t) = \frac{2\left(\omega_q^2 + \omega^2\right)\left(1 - \cos(\omega t)\cos(\omega_q t)\right) - 4\omega\omega_q \sin(\omega t)\sin(\omega_q t)}{\left(\omega^2 - \omega_q^2\right)^2} \approx \begin{cases} 4\sin^2(\omega t/2)/\omega^2 & \omega_q = 0 \\ \pi t\Big[\delta(\omega - \omega_q) + \delta(\omega + \omega_q)\Big] & \omega_q \gg 1/t \end{cases} , \tag{42}$$

and for high-frequency noise we used the conventional long-time approximation of $f(\omega, \omega_q, t)$ valid when $t \gg 1/\omega_q$.

For quasi-static noise $S_{\mathrm{QS}}(\omega) = 4\pi\eta^2\delta(\omega)$, and pink noise $S_{\mathrm{PN}}(\omega) = \eta^2/|\omega|^{1-\epsilon}$, we find, respectively,

$$\frac{\sigma_{\mathrm{QS}}^2(t)}{2} \approx \eta^2\lambda_x^2 t^2 = \frac{t^2}{T_{\mathrm{QS}}^2} , \quad \text{and} \quad \frac{\sigma_{\mathrm{PN}}^2(t)}{2} \approx \frac{\eta^2\lambda_x^2}{2\pi\epsilon}t^2 + \frac{\eta^2\omega_q}{2}t = \frac{t^2}{(T_{\mathrm{PN}}^x)^2} + \frac{t}{T_{\mathrm{PN}}^q} . \tag{43}$$

We neglect here the small contribution from the fluctuations of λ_z, which is suppressed by a factor $\sim \lambda_z^2/\omega_q^2$. Explicitly, the three time-scales are

$$T_{\mathrm{QS}} = \frac{1}{\eta\lambda_x} , \quad T_{\mathrm{PN}}^x = \frac{\sqrt{2\pi\epsilon}}{\eta\lambda_x} , \quad T_{\mathrm{PN}}^q = \frac{2}{\eta^2\omega_q} = \frac{\lambda_x^2}{\pi\omega_q\epsilon}(T_{\mathrm{PN}}^x)^2 . \tag{44}$$

We can now estimate the T_2^R in our devices. Because at $\lambda_z = 0$ and in our limited measurement-time window of $\approx 2~\mu$s, we do not observe any visible decay of our Rabi oscillations, we expect $T_2^R \gtrsim 10~\mu$s, for which we would observe a decay of the Rabi amplitude of $1 - e^{-(2/10)^2} \approx 4\%$ of the Rabi amplitude. Considering pink noise with $\epsilon = 0.1$ and $\eta = 5 \times 10^{-5}$, as discussed in Sec. II D 1, and using the measured values of $\lambda_x/2\pi = 30$ MHz and $\omega_q/2\pi = 4.5$ GHz in our current devices, we obtain $T_{\mathrm{PN}}^x \approx 85~\mu$s, and $T_{\mathrm{PN}}^q \approx 28$ ms. Pure quasi-static noise instead results in $T_{\mathrm{QS}} \approx 100~\mu$s.

The infidelity of the Rabi oscillations in the two cases is shown in Fig. 4(c). The estimates in the previous paragraph and the faster Gaussian decay caused by T_{PN}^x suggests that the dominant source of noise in our devices is the low-frequency fluctuation of λ_x. This also completely determine the Rabi decay in the quasi-static noise case $S(\omega) \propto \delta(\omega)$. This result is also qualitatively consistent with the constant value of the quality factor $Q = \lambda_x T_2^R/2\pi \approx \sqrt{2\epsilon}/2\pi\eta$ that is experimentally measured in other hole spin qubits, e.g. in germanium-silicon core-shell nanowires [7]. For this reason in the main text we focus on quasi-static noise.

We note that the value $T_2^R \approx 85~\mu$s is estimated with an upper bound of $\epsilon = 0.1$; at lower temperatures, we expect ϵ to become shorter [5], thus reducing T_2^R because $T_{\mathrm{PN}}^x \propto \sqrt{\epsilon}$, see Eq. (44). For example, at $\epsilon = 0.01$ (reported e.g. in electrons in silicon [8], and compatible with our measured temperature dependence), we find $T_2^R \approx 25~\mu$s. We also emphasize that T_2^R becomes shorter for faster Rabi oscillations. For example, at $\lambda_x/2\pi = 150$ MHz, recorded in silicon finFET qubits [5] and using $\epsilon = 0.01$, one find $T_2^R \approx 5~\mu$s. This term is suppressed by preparing the initial state to be a Floquet eigenstate, as we show next.

b. Resonant phase driving $\omega_z = \lambda_z$. A different case occurs when a pure Floquet mode is initialized. This occurs when $\omega_z = \lambda_z$ and phase and transverse driving are in-phase. In this case, pure dephasing has no influence on the system, and one obtains from Eq. (27) $P_R^N(nT) = 0$. However, we easily observe that

$$P_R^N(t) = 1 - |\langle\uparrow |u_0(t)\rangle|^2 = \langle P_R^N(t)\rangle = P_R(t), \tag{45}$$

independently of the random phase $\phi(t)$, remains unchanged upon averaging over a Gaussian distribution of phases. Thus by populating a single Floquet mode having fully developed oscillations in a period T, pure dephasing is suppressed. This suppression accounts for all the contributions $[\mathbf{h}_N^{\omega_z=\lambda_z}]_z$ in Eq. (34), including the quasi-static noise coming from fluctuations in λ_z.

This result is illustrated in Fig. 4(a), where we show how the dominant quasi-static noise source is suppressed when the resonant condition $\omega_z = \lambda_z$ is approached. We note that as expected in analogy to Bloch band theory, the suppression of Rabi oscillations requires the noise level to be below the gap, i.e. $\eta \lesssim 1$. This effect is shown in Fig. 4(b), where we use the quasi-static noise approximation to show how the opening of the gap affects the qubit decay.

4. Relaxation of Floquet modes

We now consider pure relaxation of the Floquet modes. We restrict ourselves to the case where a single Floquet mode is prepared, i.e. when the phase driving is resonant, i.e., $\omega_z = \lambda_z$. In this case, the noise originates from the x, y components of $\mathbf{h}_N^{\omega_z=\lambda_x}$ in Eq. (34); here the matrix $\mathcal{D}_{ij}^{\mathrm{rel}}(t) = e^{-i(\phi_x(t)\sigma_x + \phi_y(t)\sigma_y)/2}$.

We focus on the long-time limit such that the covariance matrix of the phases $\phi_{x,y}$ is isotropic, with diagonal components

$$\frac{\sigma^2(t)}{2} \approx \frac{1}{4\pi} \int_{-\infty}^{\infty} d\omega S_{\text{PN}}(\omega) \frac{\omega_q^2}{4} f(\omega, \lambda_x - \lambda_z, t) \approx \frac{t}{T_{\text{rel}}} \text{ , with } T_{\text{rel}} = \frac{8(\lambda_x - \lambda_z)}{\omega_q^2 \eta^2} \text{ ,} \tag{46}$$

where we consider only the largest contribution of the term proportional to ω_q. With the parameters estimated in Sec. II D 1 and for $Z = 0.3$, we find $T_{\text{rel}} \approx 530\ \mu$s. Here we also restrict ourselves to the analysis of pink noise, which gives a finite result at lowest order in perturbation theory. In particular, we note that in the case of quasi-static noise the decay rates coming from Eq. (46) vanish, but higher-order corrections in the Magnus expansion in Eq. (35), results in a finite relaxation time and in a power law decay of Rabi oscillations, see e.g. Refs. [9–11].

The Rabi probability for a single disorder realization for pure relaxation is

$$P_R^N(t) = 1 - \left| \sum_j e^{-i\omega_j^F t} \langle 0_F | u_j(t) \rangle \mathcal{D}_{j0}^{\text{rel}}(t) \right|^2 \text{ ,} \tag{47}$$

and by averaging over an isotropic Gaussian distribution we find

$$\langle P_R^N(t) \rangle = 1 - |\langle \uparrow | u_0(t) \rangle|^2 + \left(|\langle \uparrow | u_0(t) \rangle|^2 - |\langle \uparrow | u_1(t) \rangle|^2 \right) \frac{\sigma(t)}{\sqrt{2}} F\left(\frac{\sigma(t)}{\sqrt{2}} \right) \tag{48a}$$

$$= 1 - \frac{|\langle \uparrow | u_0(t) \rangle|^2| + \langle \uparrow | u_1(t) \rangle|^2}{2} + \frac{|\langle \uparrow | u_0(t) \rangle|^2 - \langle \uparrow | u_1(t) \rangle|^2}{2\sigma^2(t)} + \mathcal{O}(\sigma^{-3}) \text{ .} \tag{48b}$$

Here $F(x)$ is the Dawson function; we expanded it in the long-time limit, where Eq. (46) holds. At the stroboscopic times nT and for large n, $\langle P_R^N(nT) \rangle \to 1/2$ as expected, and, interestingly, the attenuation caused by relaxation is a power-law decay $\propto 4T_{\text{rel}}/t$. We note that a similar relaxation-induced power-law decay $\propto 1/\sqrt{1 + (4t/T_{\text{rel}})^2} \to 4T_{\text{rel}}/t$ also appears for quasi-static noise in the conventional Rabi oscillations [9–11].

The relaxation contribution to T_2^R is plotted (via the fidelity) in Fig. 4(c) along with other sources. In our current devices, relaxation results in ~ 10 times slower decay of oscillations. Because the dominant contribution to dephasing $T_2^R \propto \sqrt{\epsilon}/\lambda_x$, see Eq. (43), becomes shorter for larger λ_x and for pure $1/\omega$ noise, we expect relaxation to be increasingly negligible for faster qubits.

[1] S. Bosco, P. Scarlino, J. Klinovaja, and D. Loss, Fully tunable longitudinal spin-photon interactions in si and ge quantum dots, Phys. Rev. Lett. **129**, 066801 (2022).

[2] M. Bukov, L. D'Alessio, and A. Polkovnikov, Universal high-frequency behavior of periodically driven systems: from dynamical stabilization to floquet engineering, Advances in Physics **64**, 139 (2015), https://doi.org/10.1080/00018732.2015.1055918.

[3] D. Zeuch, F. Hassler, J. J. Slim, and D. P. DiVincenzo, Exact rotating wave approximation, Annals of Physics **423**, 168327 (2020).

[4] F. Vigneau, F. Fedele, A. Chatterjee, D. Reilly, F. Kuemmeth, M. F. Gonzalez-Zalba, E. Laird, and N. Ares, Probing quantum devices with radio-frequency reflectometry, Applied Physics Reviews **10**, 021305 (2023), https://pubs.aip.org/aip/apr/article-pdf/doi/10.1063/5.0088229/17368125/021305_1_5.0088229.pdf.

[5] L. C. Camenzind, S. Geyer, A. Fuhrer, R. J. Warburton, D. M. Zumbühl, and A. V. Kuhlmann, A hole spin qubit in a fin field-effect transistor above 4 kelvin, Nature Electronics 10.1038/s41928-022-00722-0 (2022).

[6] L. Cywiński, R. M. Lutchyn, C. P. Nave, and S. Das Sarma, How to enhance dephasing time in superconducting qubits, Phys. Rev. B **77**, 174509 (2008).

[7] F. N. M. Froning, L. C. Camenzind, O. A. H. van der Molen, A. Li, E. P. A. M. Bakkers, D. M. Zumbühl, and F. R. Braakman, Ultrafast hole spin qubit with gate-tunable spin–orbit switch functionality, Nature Nanotechnology **16**, 308 (2021).

[8] J. Yoneda, K. Takeda, T. Otsuka, T. Nakajima, M. R. Delbecq, G. Allison, T. Honda, T. Kodera, S. Oda, Y. Hoshi, N. Usami, K. M. Itoh, and S. Tarucha, A quantum-dot spin qubit with coherence limited by charge noise and fidelity higher than 99.9%, Nature Nanotechnology **13**, 102 (2018).

[9] F. H. L. Koppens, D. Klauser, W. A. Coish, K. C. Nowack, L. P. Kouwenhoven, D. Loss, and L. M. K. Vandersypen, Universal phase shift and nonexponential decay of driven single-spin oscillations, Phys. Rev. Lett. **99**, 106803 (2007).

[10] J. Fischer, W. A. Coish, D. V. Bulaev, and D. Loss, Spin decoherence of a heavy hole coupled to nuclear spins in a quantum dot, Phys. Rev. B **78**, 155329 (2008).

[11] S. Bosco and D. Loss, Fully tunable hyperfine interactions of hole spin qubits in si and ge quantum dots, Phys. Rev. Lett. **127**, 190501 (2021).